ISSN 0869-5911, Petrology, 2006, Vol. 14, No. 1, pp. 98–114. © Pleiades Publishing, Inc., 2006.
Original Russian Text © G.G. Lepezin, A.V. Travin, D.S. Yudin, N.I. Volkova, A.V. Korsakov, 2006, published in Petrologiya, 2006, Vol. 14, No. 1, pp. 109–125.

Age and Thermal History of the Maksyutov Metamorphic Complex: $^{40}Ar/^{39}Ar$ Evidence

G. G. Lepezin*, A. V. Travin, D. S. Yudin**, N. I. Volkova*, and A. V. Korsakov***

** Institute of Mineralogy and Petrography, Siberian Division, Russian Academy of Sciences, pr. Akademika Koptyuga 3, Novosibirsk, 630090 Russia*
e-mail: lepezin@uiggm.nsc.ru
***United Institute of Geology, Geophysics, and Mineralogy, Siberian Division, Russian Academy of Sciences, pr. Akademika Koptyuga 3, Novosibirsk, 630090 Russia*
e-mail: travin@uiggm.nsc.ru

Received October 10, 2004

Abstract—The $^{40}Ar/^{39}Ar$ method with stepwise heating was used to date phengite and glaucophane in the contact zone of garnet glaucophanite an omphacite–garnet rock (eclogite) from the lower unit of the Maksyutov metamorphic complex. The correlation of the measured age and the sizes of the phengite flakes indicates that the behavior of radiogenic Ar in them was controlled by the mechanisms of volumetric diffusion. Taking into account the fact that all of the rocks have the same thermal history, the dates most close to the age of metamorphism are those of the largest phengite flakes from garnet glaucophanite: 392 Ma. The age values obtained on phengite from an omphacite–garnet rock sampled at the maximum distance from the contact are equal to 378 Ma and correspond to the time when the rocks cooled to temperatures below 350°C. The results of numerical simulations indicate that the metamorphic age is no younger than 400 Ma, and the linear cooling rate can be estimated at 3.40 –0.75/+1.24°C/m.y. The maximum values of the phengite ages are consistent with the dates of glaucophane from three rock samples: 389–411 Ma.

DOI: 10.1134/S0869591106010085

INTRODUCTION

Complexes of glaucophane schists and eclogites with glaucophane schists in the Ural–Mongolia Foldbelt mark its major sutures—collision zones—and can be reliable indicators of the principal collision stages (Dobretsov, 2003), which predetermines acute interest in these rocks. The Uralian orogen was produced by the oblique collision of the East European Platform and a variety of microcontinents in the Late Paleozoic (Zonenshain *et al.*, 1984; Dobretsov *et al.*, 1996; Puchkov, 1997). The early collision stage was responsible for the origin of the Maksyutov metamorphic complex in the Southern Urals. The complex extends in the meridional direction for more than 200 km as a 15- to 20-km-wide stripe, is bounded, along the Main Ural Fault, by the hyperbasites of the Kempirsai Belt in the east, and is tectonically juxtaposed with the Lower Paleozoic platform sedimentary cover in the west. The complex consists of two units: the lower one is made up of various schists, including those with glaucophane, with beds of quartzites and numerous boudins of eclogites, garnet–omphacite, and olivine–enstatite rocks; whereas the upper unit is dominated by metagraywackes and graphite-bearing schists with bodies of serpentinites, metabasalts, and metagabbro.

The mineral assemblages, compositions of minerals, and mineralogical thermometric data indicate that the rocks of the lower unit were metamorphosed at P = 15–23 kbar and T = 550–700°C (Beane *et al.*, 1995; Lennykh *et al.*, 1995; Dobretsov *et al.*, 1996; Hetzel *et al.*, 1998; Schulte and Blümel, 1999; Volkova *et al.*, 2004). With regard for the occurrence of quartz pseudomorphs after coesite (Chesnokov and Popov, 1965; Dobretsov and Dobretsov, 1988) and graphite cuboids after diamond (Leech and Ernst, 1998), the pressure during the early metamorphic stage could have reached 27–32 kbar.

Isotopic dates for various rocks and minerals from this complex are listed in Table 1. They were obtained by various methods and constrain the age interval to 390–365 Ma. The average $^{40}Ar/^{39}Ar$ phengite age of the eclogites is t_{av} = 374.4 Ma (four samples, t_{max} = 375.4 Ma, t_{min} = 372.9 Ma); the Rb/Sr phengite and whole-rock age of the rocks is t_{av} = 375.1 Ma (nine samples, t_{max} = 378.5 Ma, t_{min} = 372.0 Ma); the U/Pb rutile concordia ages are equal to 377 ± 2– 384 ± 4 Ma; the Sm–Nd garnet, phengite, pyroxene, amphibole, and whole-rock ages range from 366 ± 7 to 378 ± 13 Ma; and the U/Pb zircon dating by SHRIMP is 387.5 ± 4.1 Ma. The $^{40}Ar/^{39}Ar$ phengite age of the glaucophane schists was determined to be constrained between 377.7 ± 3.8 and 387.9 ± 4.0 Ma. The ages of other rocks vary from 365 ± 2 Ma (quartzites) to 377 ± 2 Ma (graphite-bearing schists). It should be mentioned that 21 of the 26 isotopic dates pertain to the eclogites, and only two

Table 1. Review of isotopic dates obtained for high-pressure rocks of the lower unit of the Maksyutov Complex (literature data)

Mineral	Method	Age*, Ma	Reference
	Eclogite		
phengite	$^{40}Ar/^{39}Ar$, plateau	372.9 ± 3.8	Matte *et al.*, 1993
phengite	$^{40}Ar/^{39}Ar$, plateau	375.4 ± 3.4	Lennykh *et al.*, 1995
white mica	$^{40}Ar/^{39}Ar$, plateau	374 ± 4	Beane and Connelly, 2000
phengite	$^{40}Ar/^{39}Ar$, plateau	375 ± 4	Beane and Connelly, 2000
phengite	$^{40}Ar/^{39}Ar$, plateau	374 ± 3	Beane and Connelly, 2000
phengite, glaucophane, omphacite	Rb/Sr, isochron	376.5 ± 3.7	Glodny *et al.*, 2002
phengite, paragonite	Rb/Sr, isochron	378.5 ± 4.7	Glodny *et al.*, 2002
phengite, epidote, apatite	Rb/Sr, isochron	375.2 ± 3.8	Glodny *et al.*, 2002
phengite, epidote, glaucophane, omphacite, whole rock	Rb/Sr, isochron	372.4 ± 3.8	Glodny *et al.*, 2002
phengite, glaucophane, omphacite, whole rock	Rb/Sr, isochron	375.5 ± 2.2	Glodny *et al.*, 2002
phengite, epidote, glaucophane, omphacite, whole rock	Rb/Sr, isochron	373.8 ± 3.9	Glodny *et al.*, 2002
phengite, paragonite	Rb/Sr, isochron	372 ± 15	Glodny *et al.*, 2002
phengite, omphacite, paragonite	Rb/Sr, isochron	377.7 ± 7.3	Glodny *et al.*, 2002
phengite, omphacite, apatite	Rb/Sr, isochron	374.3 ± 2.7	Glodny *et al.*, 2002
rutile, apatite	U/Pb, $^{206}Pb/^{204}Pb$–$^{238}U/^{204}Pb$ isochron	377 ± 2	Beane and Connelly, 2000
rutile, apatite	U/Pb, $^{206}Pb/^{204}Pb$–$^{238}U/^{204}Pb$ isochron	384 ± 3	Beane and Connelly, 2000
zircon	U/Pb SHRIMP, Tera–Waserburg concordia	387.5 ± 4.1	Leech *et al.*, 2002
rutile, apatite, garnet, clinopyroxene	Sm/Nd, isochron	399 ± 35	Beane and Connelly, 2000
rutile, apatite	Sm/Nd, isochron	382 ± 10	Beane and Connelly, 2000
omphacite, garnet, epidote	Sm/Nd, isochron	416 ± 26	Glodny *et al.*, 2002
phengite, pyroxene, garnet, amphibole, whole rock	Sm/Nd, isochron	378 ± 13	Shatsky *et al.*, 1997
	Glaucophane schist		
phengite	$^{40}Ar/^{39}Ar$, plateau	377.7 ± 3.8	Matte *et al.*, 1993
phengite	$^{40}Ar/^{39}Ar$, plateau	387.9 ± 4.0	Matte *et al.*, 1993
	Other rocks		
white mica (mica schist)	$^{40}Ar/^{39}Ar$, plateau	372 ± 2	Beane and Connelly, 2000
phengite (graphite schist)	$^{40}Ar/^{39}Ar$, plateau	377 ± 2	Beane and Connelly, 2000
phengite (quartzite)	$^{40}Ar/^{39}Ar$, plateau	365 ± 2	Beane and Connelly, 2000

* Errors are reported for ±2σ intervals.

dates were obtained for the glaucophane schists. In spite of the great number of the isotopic dates, there is still no consensus on the age of the high-pressure metamorphism. Difficulties in the interpretation of the isotopic dates are explained by the fact that the rocks composing this complex were partly affected by younger overprinted metamorphism of the blue- and greenschist facies.

The generalization of geochronological data and fission-track apatite dates made it possible to estimate the exhumation velocity of the complex at 0.3–1.5 mm/yr (Leech and Stockli, 2000).

This publication is devoted to the $^{40}Ar/^{39}Ar$ dating of phengite and glaucophane that were sampled within the contact zone of chemically contrasting rocks—garnet glaucophanite and an omphacite–garnet rock in the lower unit of the Maksyutov metamorphic complex—and to the analysis of the thermal history of these rocks.

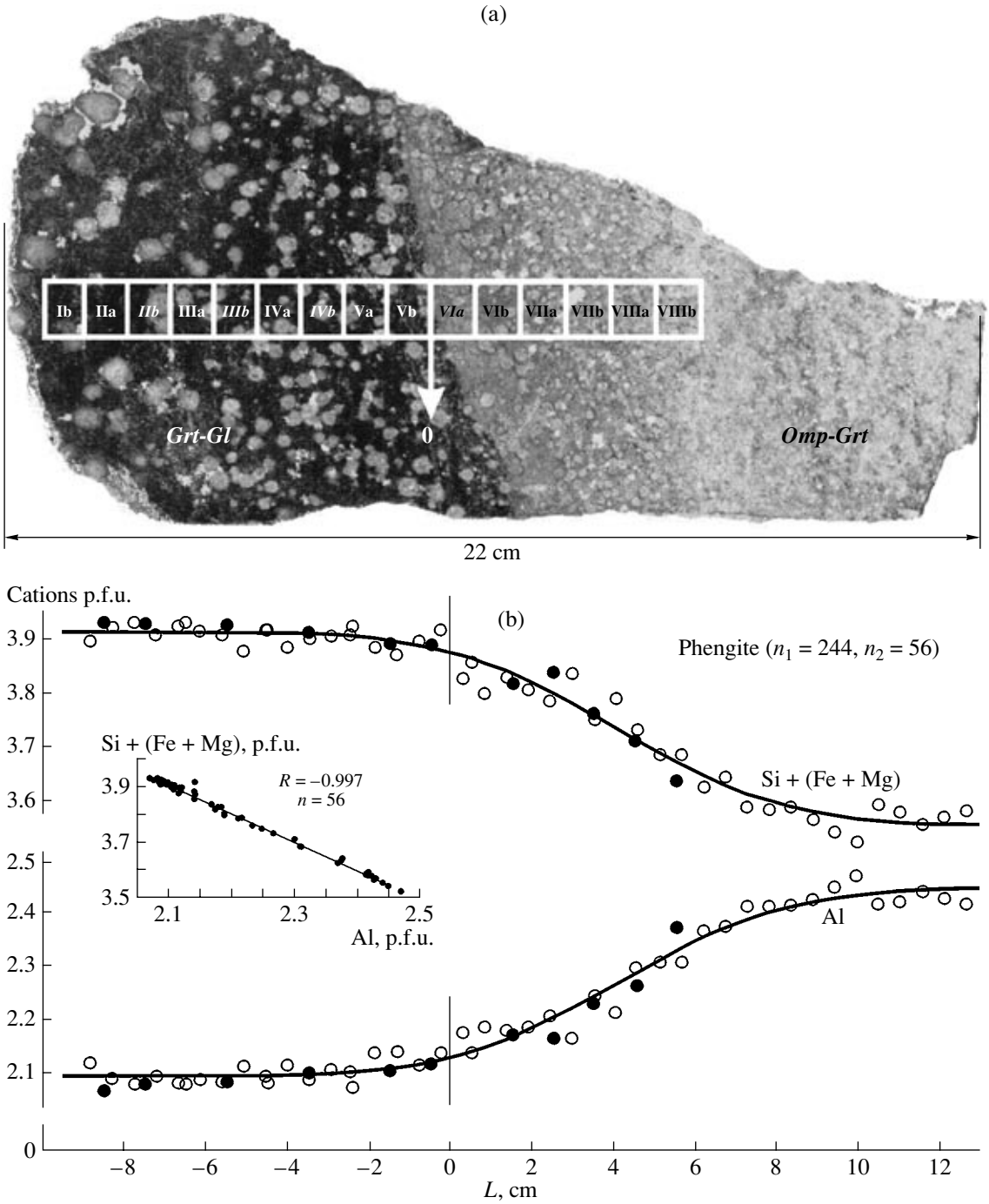

Fig. 1. (a) Photograph of the specimen with marked phengite sampling sites (written in italics are samples that were not dated isotopically). *Grt–Gl* is garnet glaucophanite, *Omp–Grt* is omphacite–garnet rock.
(b) Dependence of the concentrations of Al and Si + (Mg + Fe) in phengite on the distance of the sampling site from the contact *L*; n_1 is the total number of analyses, n_2 is the number of averaged analyses. Solid circles correspond to samples that were dated isotopically. The inset shows the correlation between the concentrations of Al and Si + (Mg + Fe) in phengite, *R* is the correlation coefficient.

METHODS

This research was conducted using a single sample from the contact zone of garnet glaucophanite and an omphacite–garnet rock. A platelet (22 × 11 × 1 cm, Fig. 1a) cut out of this rock was, in turn, used to prepare a series of petrographic thin sections oriented perpendicular to the contact. The compositions of garnet (rim–core–rim), omphacite, glaucophane, and phengite were analyzed in these thin sections on a CAMEBAX Micro (Cameca, France) microprobe.

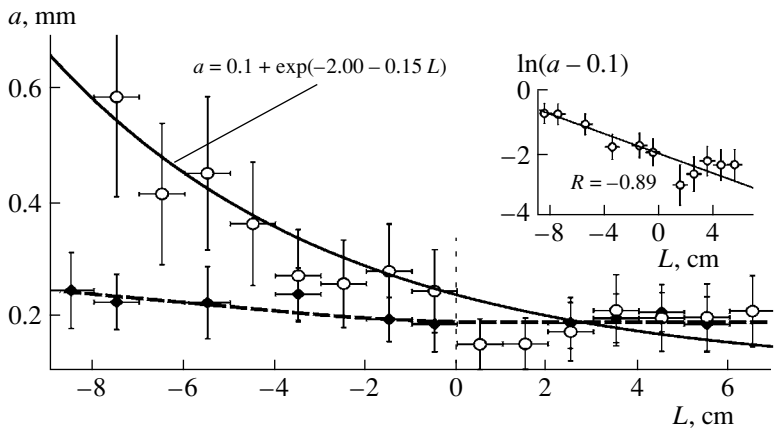

Fig. 2. Dependence of the half-lengths of the short axes of phengite flakes a on the distance from the rock contact L.
Open circles show measurements in thin sections, solid diamonds are measurements in the monomineralic fraction separated for $^{40}Ar/^{39}Ar$ isotopic research. The inset shows the correlation of ln $(a - 0.1)$ and the distance from the rock contact (measurements in thin sections); R is the correlation coefficient.

In addition, the compositions of phengite and glaucophane were determined in grains from crushed samples, which were sampled along a profile perpendicular to the contact, with sampling sites spaced 3–5 mm apart. The analyses were conducted in 5–7 grains, each analyzed at no less than five spots, with the subsequent averaging of the analyses (Table 2). The sizes of phengite flakes were measured in thin sections along their long and short axes and in each monomineralic fraction used for isotopic dating.

Phengite and glaucophane for $^{40}Ar/^{39}Ar$ dating were separated from a series of 1-cm cubes that were cut out of the rock perpendicular to the contact (Fig. 1a). Then these samples were wrapped, along with biotite monomineralic samples MCA-11 and LP-6 that were used as flux monitors, in aluminum foil, placed in a quartz ampoule, which was welded upon air evacuation. The samples were then irradiated in the Cd-shielded carrier of the VVR-K research reactor at the Tomsk Polytechnic Institute. The neutron flux gradient did not exceed 0.5% of the sample size. The stepwise heating experiments were conducted in a quartz reactor with an external furnace. The blank did not exceed 5×10^{-10} ncm^3 for ^{40}Ar (10 min at 1200°C). The argon was purified at Ti and ZrAl SAES getters. The Ar isotopic composition was measured on a Noble gas 5400 (Micromass, Great Britain) mass spectrometer. The measurement errors quoted below in the text, tables (except Table 1), and figures correspond to $\pm 1\sigma$.

RESULTS AND DISCUSSION

The omphacite–garnet rock (eclogite) consisted of ~30% quartz, ~25% omphacite, ~15% phengite, ~5% glaucophane, ~5% actinolite, ~5% albite, and accessory amounts of sphene and rutile. The garnet glaucophanite was made up of ~40% glaucophane, ~20% garnet, ~20% quartz, ~10% phengite, ~5% actinolite, with no rutile, sphene, and omphacite.

The metamorphic parameters of the rock were evaluated by a variety of mineralogical thermobarometers and the THERMOCALC computer package (Holland and Powell, 1998) at spots located at various distances from the contact. The calculations were carried out with the compositions of coexisting glaucophane, garnet, and phengite for the garnet glaucophanite and with the compositions of omphacite, garnet, and phengite for the omphacite–garnet rock. Inasmuch all garnet grains were chemically heterogeneous, we used the compositions of their cores and rims. The ranges of the average temperature and pressure estimates were T = 450–600°C and P = 18–26 kbar.

The rocks in question are not in chemical equilibrium and show reaction relations. The thickness of the diffusion exchange zone, which was estimated from the distribution of the concentrations of selected components of the rocks and minerals (garnet, glaucophane, and phengite), was 5–15 cm. The maximum thicknesses of this zone were typically yielded by phengite. The Al and Si + (Fe + Mg) profiles constructed for phengite are complementary (Fig. 1b). This is explained by the character of isomorphism in this mineral and the negative correlation of phengite components with extremely high values of R = –0.997 (Fig. 1b, inset).

The concentration of the celadonite end member in phengite from the garnet glaucophanite is practically constant and not correlated with the distance from the contact (L) and, conversely, systematically varies in this mineral from the omphacite–garnet rock depending on L (Fig. 1b). The sizes of phengite flakes in the latter rock are weakly correlated with the distance L and increase with increasing L for this mineral from the garnet glaucophanite (Fig. 2). The sizes of phengite flakes

Table 2. Chemical composition and flake sizes of phengite and chemical composition of glaucophane

Sample	*L*, cm	Size*, mm		Chemical composition, wt %								Numbers of cations per formula units of phengite (per 11 O) and glaucophane (per 23 O)							
		$a \pm 1\sigma$	$b \pm 1\sigma$	SiO_2	Al_2O_3	FeO**	MgO	CaO	Na_2O	K_2O	Total	Si	Al	Fe	Mg	Ca	Na	K	Total
Phengite, garnet glaucophanite																			
I	−8.5	0.599 ± 0.177	3.973 ± 1.192	51.34	26.46	2.54	3.78	–	0.46	10.08	94.66	3.42	2.07	0.14	0.37	–	0.06	0.85	6.91
IIa	−7.5	0.588 ± 0.176	3.973 ± 1.192	51.04	26.41	2.51	3.75	–	0.50	10.15	94.36	3.42	2.08	0.14	0.37	–	0.07	0.87	6.95
IIb	−6.5	0.416 ± 0.125	2.787 ± 0.836	51.22	26.44	2.48	3.70	–	0.47	10.07	94.38	3.43	2.08	0.14	0.37	–	0.06	0.86	6.94
IIIa	−5.5	0.453 ± 0.136	2.174 ± 0.652	50.85	26.35	2.37	3.74	–	0.44	10.15	93.9	3.42	2.09	0.13	0.37	–	0.06	0.87	6.94
IIIb	−4.5	0.363 ± 0.109	1.748 ± 0.524	50.99	26.44	2.49	3.68	–	0.48	9.96	94.04	3.41	2.09	0.14	0.37	–	0.06	0.85	6.91
IVa	−3.5	0.272 ± 0.081	1.067 ± 0.320	50.69	26.38	2.41	3.66	–	0.52	10.08	93.74	3.41	2.09	0.14	0.37	–	0.07	0.86	6.94
IVb	−2.5	0.257 ± 0.077	1.061 ± 0.318	50.40	26.52	2.47	3.73	–	0.55	10.01	93.68	3.40	2.11	0.14	0.37	–	0.07	0.86	6.94
Va	−1.5	0.279 ± 0.084	0.863 ± 0.259	50.78	26.74	2.39	3.62	–	0.57	10.06	94.16	3.40	2.11	0.13	0.36	–	0.07	0.86	6.93
Vb	−0.5	0.244 ± 0.073	0.688 ± 0.206	50.91	26.82	2.55	3.33	–	0.45	10.17	94.23	3.42	2.12	0.14	0.33	–	0.06	0.87	6.94
Phengite, omphacite–garnet rock																			
VIa	0.5	0.150 ± 0.045	0.314 ± 0.094	50.72	27.15	2.44	3.26	–	0.52	10.17	94.26	3.40	2.14	0.14	0.32	–	0.07	0.87	6.94
VIb	1.5	0.151 ± 0.045	0.326 ± 0.098	50.19	27.55	2.34	3.28	–	0.58	10.01	93.95	3.36	2.18	0.13	0.33	–	0.07	0.86	6.93
VIIa	2.5	0.173 ± 0.052	0.293 ± 0.088	50.54	27.46	2.33	3.22	–	0.55	10.03	94.13	3.39	2.17	0.13	0.32	–	0.07	0.86	6.94
VIIb	3.5	0.210 ± 0.063	0.263 ± 0.079	50.06	28.56	2.25	2.82	–	0.66	9.94	94.29	3.35	2.25	0.13	0.28	–	0.09	0.85	6.95
VIIIa	4.5	0.197 ± 0.059	0.238 ± 0.071	49.60	29.25	2.26	2.76	–	0.67	9.73	94.27	3.31	2.30	0.13	0.27	–	0.09	0.83	6.93
VIIIb	5.5	0.198 ± 0.059	0.236 ± 0.071	49.57	30.35	2.16	2.27	–	0.75	9.52	94.62	3.29	2.30	0.13	0.27	–	0.10	0.81	6.90
Glaucophane, garnet glaucophanite																			
I	−8.5	–	–	56.60	11.83	10.49	9.83	0.73	7.23	0.06	96.77	7.87	1.94	1.22	2.04	0.11	1.95	0.01	15.14
IIIa	−5.5	–	–	57.37	12.05	10.31	10.00	0.68	7.10	0.04	97.55	7.89	1.95	1.19	2.05	0.10	1.89	0.01	15.08
IVa	−3.5	–	–	57.57	12.05	10.33	9.69	0.55	7.21	0.03	97.43	7.92	1.96	1.19	1.99	0.08	1.92	0.01	15.07
Vb	−0.5	–	–	57.33	11.56	10.74	9.22	0.38	7.01	0.02	96.26	7.99	1.90	1.25	1.91	0.06	1.89	0.00	15.00

Note: *L* is the distance from the rock contact;
* measurements in thin sections: *a* is the half-length of the short axis, *b* is the half-length of the long axis (no less than 30 measurements);
** all Fe as FeO.

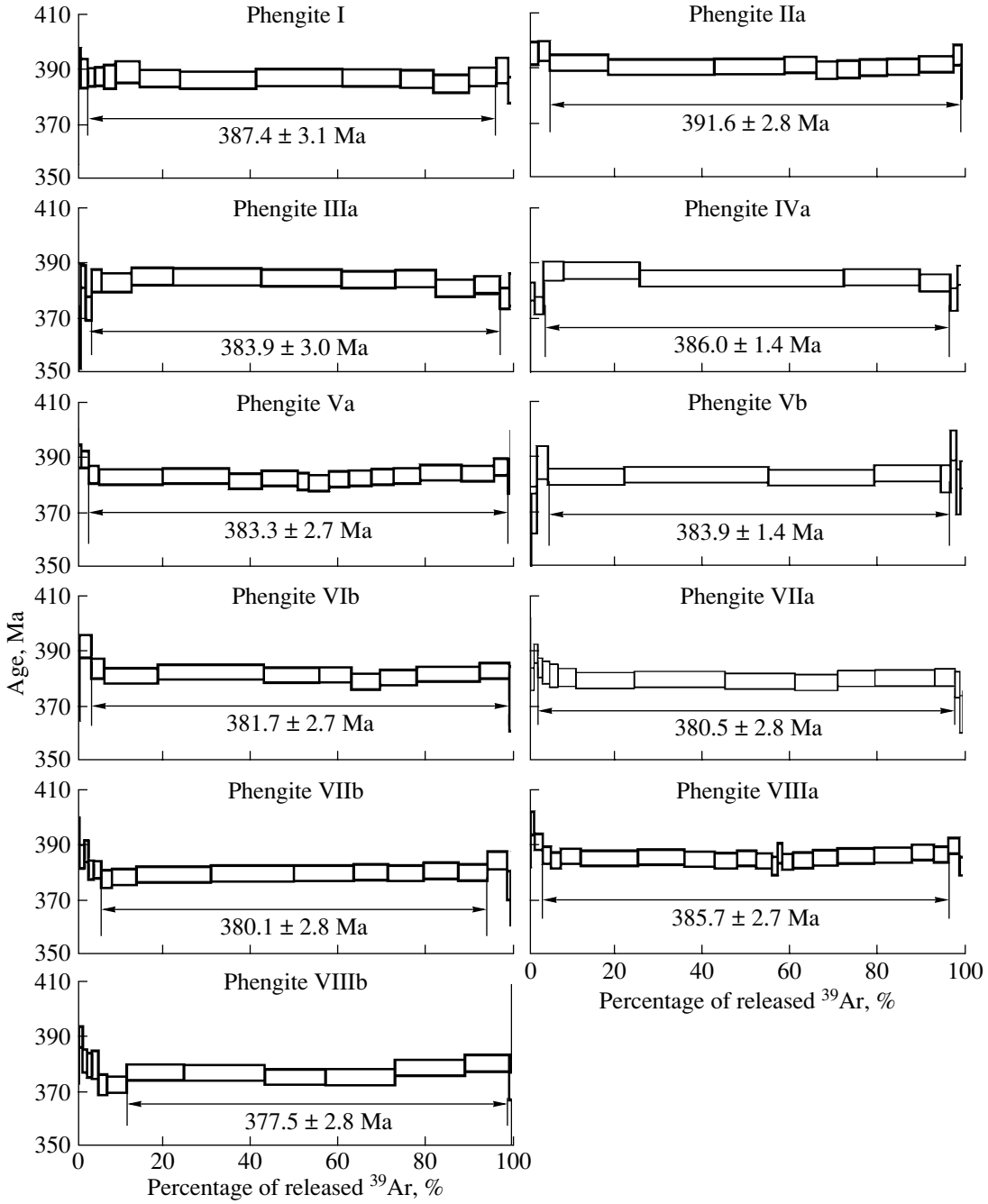

Fig. 3. Results of the $^{40}Ar/^{39}Ar$ study of phengite. Age spectra are presented for each sample.

from the omphacite–garnet rock measured in the monomineralic factions for isotopic dating coincide with the flake sizes in thin sections and are much smaller than the sizes of phengite flakes in thin sections of the garnet glaucophanite. This suggests that phengite flakes were broken and diminished in size during their separation. Because of this, the further calculations and modeling with the use of isotopic data were conducted with data on the variations in the phengite flake sizes measured in thin sections.

Figures 3 and 4 and Tables 3–5 presents the results of the $^{40}Ar/^{39}Ar$ dating. The spectra of all phengite and glaucophane I samples show a clearly pronounced age plateau. The spectra of glaucophane IIIa, IVa, and Vb display plateaus at two levels, which correspond to more than 80% of the released ^{40}Ar. The age of the phengite plateau for the whole sampling varies from 392 to 379 Ma, and the age of glaucophane plateaus ranges from 449 to 387 Ma. It is pertinent to mention that the age values obtained using the plateau method

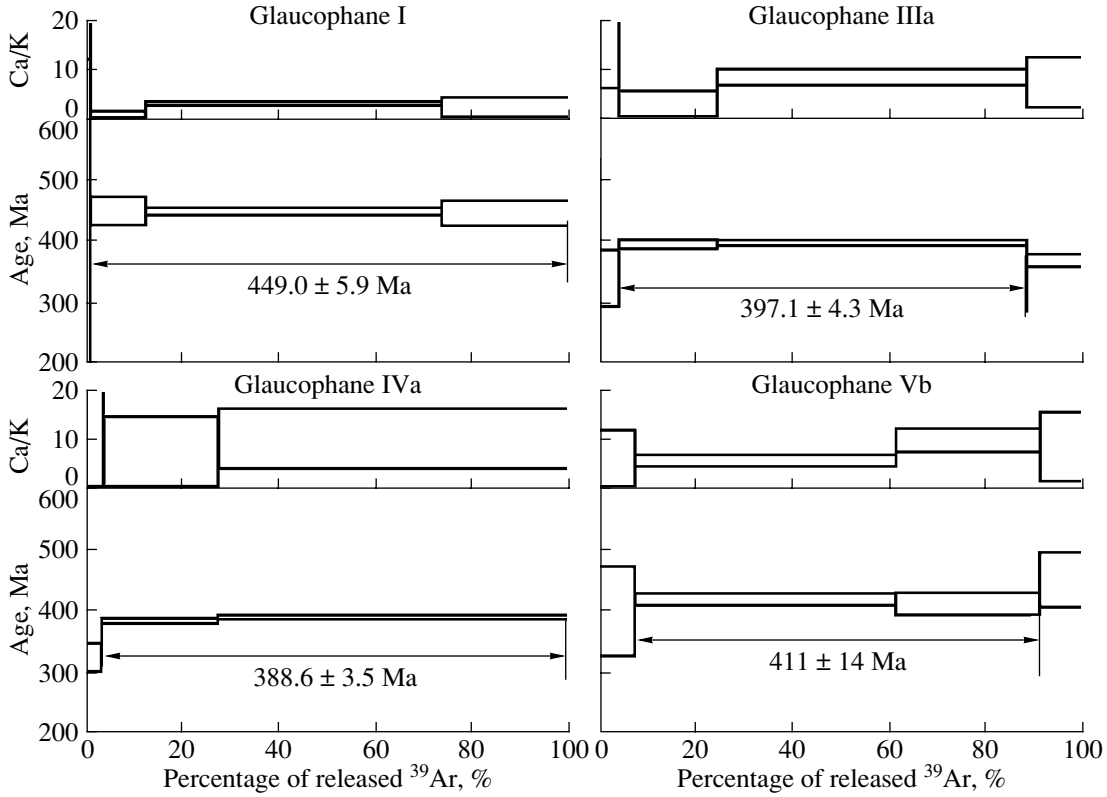

Fig. 4. Results of the ^{40}Ar/^{39}Ar study of glaucophane. Age and Ca/K spectra are presented for each sample.

with an isochron regression and the integral technique coincide, within the analytical errors, for all of the samples (Table 3). In spite of the significant scatter of the dates, the internal criteria of the ^{40}Ar/^{39}Ar method (isochron regression and the configuration of the age spectrum) do not suggest the presence of excess radiogenic argon in the minerals. The isochron age is determined with an error greater than the total fusion and plateau ages. The total fusion age is contributed by low-temperature levels, which are characterized by age values lower or higher than that of the plateau. This means that the dates calculated by the plateau method are maximally close to the closure age of the K/Ar systems of the minerals.

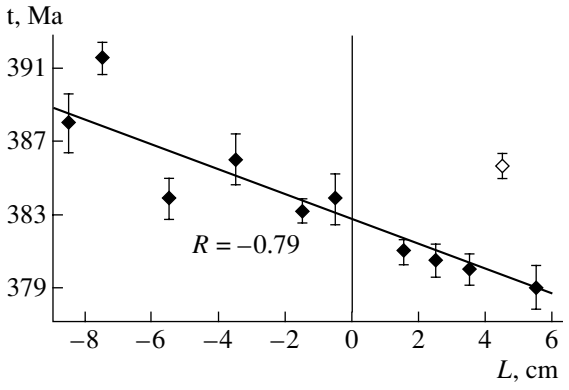

Fig. 5. Dependence of the measured ^{40}Ar/^{39}Ar age of phengite on the distance from the rock contact *L*. The open diamond corresponds to the data point rejected from the calculation of correlation coefficient as an anomalous sample.

The measured phengite age systematically increases from 378.9 Ma in the omphacite–garnet rock to 391.6 Ma in the garnet glaucophanite at the maximum distance from the contact (Table 3, Fig. 5). Bearing in mind that the mineral assemblages of both rocks had the same thermal history, the variations in the measured phengite age could be caused by the kinetics of Ar behavior as a function of the chemistry of this mineral, the sizes of its flakes, and the intensity and duration of overprinted thermal events, as well as the cooling rate.

The sizes of phengite flakes systematically vary with distance from the rock contact (Fig. 2): the flakes are the largest in the garnet glaucophanite (a_{max} = 0.776 mm) and the smallest in the omphacite–garnet rock (a_{min} = 0.10 mm). In a diagram showing the correlation between the sizes of the flakes and measured age (Fig. 6), the phengite points define a linear trend with a correlation coefficient of 0.92. The dependence of the age on the flake sizes can be expressed by the equation

$$t = 377.6 \pm 1.5 + 19.6 \pm 4.3a.$$

At the same time, the diagram displaying the correlation between the Al concentration and measured age

Table 3. Results of $^{40}Ar/^{39}Ar$ dating and the sizes of phengite flakes in the samples

Sample	*L*,cm	Number of steps	Isochron age, Ma	Total fusion age, Ma	Plateau age, Ma	Average age, Ma	Size, mm (number of measurements)	
							$a \pm 1\sigma$	$b \pm 1\sigma$
Phengite I	–8.5	17	386.9 ± 3.8	386.9 ± 3.1	387.8 ± 3.1	387.2	0.246 ± 0.067 (100)	0.358 ± 0.100 (100)
Glaucophane I	–8.5	4	453.1 ± 15.8	447.5 ± 8.0	449.0 ± 5.9	449.9	–	–
Phengite IIa	–7.5	16	389.7 ± 3.3	391.1 ± 2.7	391.6 ± 2.8	390.8	0.225 ± 0.049 (70)	0.321 ± 0.076 (70)
Phengite IIIa	–5.5	17	385.7 ± 3.4	383.4 ± 3.0	383.9 ± 3.0	384.3	0.224 ± 0.064 (100)	0.320 ± 0.077 (100)
Omphacite IIIa	–5.5	5	404.7 ± 8.2	390.2 ± 4.8	397.1 ± 4.3	397.3	–	–
Phengite IVa	–3.5	12	384.1 ± 3.5	384.9 ± 2.9	386.0 ± 2.9	385.0	0.239 ± 0.046 (70)	0.341 ± 0.088 (70)
Omphacite IVa	–3.5	4	397.9 ± 5.6	387.9 ± 3.7	388.6 ± 3.5	391.5	–	–
Phengite Va	–1.5	20	382.2 ± 3.0	383.6 ± 2.3	383.2 ± 2.7	383.0	0.194 ± 0.039 (70)	0.288 ± 0.063 (70)
Omphacite Vb	–0.5	4	395.6 ± 29.7	422.2 ± 17.3	411.1 ± 13.8	409.6	–	–
Phengite Vb	–0.5	11	384.5 ± 4.1	383.7 ± 2.8	383.9 ± 2.9	384.0	0.186 ± 0.049 (70)	0.255 ± 0.067 (70)
Phengite VIb	1.5	13	382.1 ± 3.2	382.1 ± 2.4	381.7 ± 2.7	382.0	–	–
Phengite VIIa	2.5	19	380.4 ± 3.1	381.1 ± 2.8	380.5 ± 2.8	380.7	0.188 ± 0.045 (70)	0.270 ± 0.069 (70)
Phengite VIIb	3.5	20	379.9 ± 3.1	380.1 ± 2.8	380.1 ± 2.8	380.0	0.196 ± 0.043 (70)	0.284 ± 0.064 (70)
Phengite VIIIa	4.5	25	385.9 ± 3.0	386.1 ± 2.7	385.7 ± 2.7	385.9	0.207 ± 0.035 (70)	0.278 ± 0.054 (70)
Phengite VIIIb	5.5	16	379.7 ± 3.2	378.5 ± 2.7	378.9 ± 2.8	379.0	0.186 ± 0.049 (100)	0.258 ± 0.075 (100)

Note: *L* is the distance from the rock contact, *a* is the half-length of the short axis, *b* is the half-length of the long axis, average ages are arithmetic mean values of isochron, total fusion, and plateau age values.

(Fig. 7) demonstrates that the variations in the Al concentration from 2.1 to 2.3 p.f.u. in phengite with an average size of flakes equal to 0.18 mm correspond to variations in the age of the omphacite–garnet rock by 5 m.y. These correlations can hardly be explained by the presence of captured radiogenic Ar in the phengite. Conversely, these correlations provide unambiguous evidence for the heterogeneous redistribution of radiogenic Ar within individual flakes and for a diffusion-controlled mechanism of Ar migration.

Since the measured age of phengite depends on its chemical composition and the sizes of its flakes, it is logical to take into account the contributions of these parameters in the following multiple regression equation:

$$t = 425.9 + 13.0a - 21.5Al,$$

where *a* is the half-length of the short axis of the flakes, and Al is the Al concentration. This equation satisfactorily describes the experimental data, because the reproducibility error $S = 1.6$ m.y. is much smaller than the errors of the Ar–Ar dates (Table 3). Substituting the sizes of phengite flakes and their compositions into the

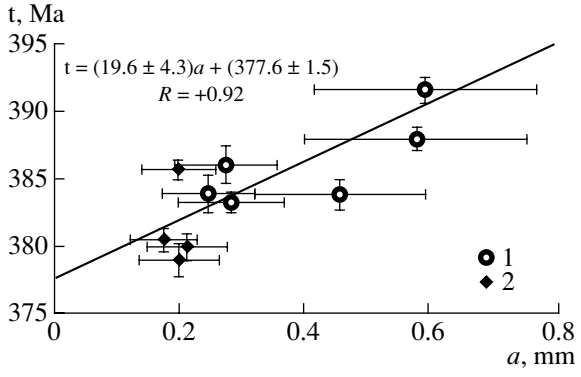

Fig. 6. Dependence of the measured $^{40}Ar/^{39}Ar$ age of phengite on the size of its flakes in thin sections.
(1) Garnet glaucophanite; (2) omphacite–garnet rock.

Table 4. Results of $^{40}Ar/^{39}Ar$ phengite dating

no.	*T*, °C	*t*, min	^{40}Ar, 10^{-9} ncm^3	$^{40}Ar/^{39}Ar$	$^{38}Ar/^{39}Ar$	$^{36}Ar/^{39}Ar$	$\Sigma^{39}Ar$, %	Age, Ma (±1σ)
Sample I, $J = 0.003379 \pm 0.000030$								
1	450	20	3.64	209.88	0.129	0.9468	0.1	365.6 ± 9.4
2	550	20	10.18	93.28	0.049	0.0905	0.4	365.6 ± 9.4
3	600	20	18.49	84.13	0.034	0.0413	1.1	392.1 ± 5.9
4	650	20	38.17	78.60	0.019	0.0249	2.6	388.8 ± 5.3
5	675	20	41.33	77.22	0.016	0.0212	4.3	387.4 ± 3.3
6	700	20	50.16	77.86	0.020	0.0232	6.3	387.7 ± 3.4
7	725	20	66.67	77.21	0.022	0.0211	9.0	387.5 ± 4.3
8	750	20	132.94	75.54	0.017	0.0142	14.5	389.3 ± 4.0
9	775	20	221.19	74.70	0.016	0.0130	23.7	386.9 ± 3.1
10	800	20	406.90	73.03	0.016	0.0078	41.1	386.4 ± 3.1
11	825	20	457.89	72.56	0.015	0.0055	60.8	387.3 ± 3.1
12	850	20	311.09	73.05	0.016	0.0072	74.1	387.2 ± 3.1
13	875	20	177.16	73.71	0.015	0.0098	81.6	386.8 ± 3.2
14	900	20	192.26	73.54	0.017	0.0104	89.7	385.0 ± 3.2
15	950	20	147.00	73.39	0.017	0.0081	96.0	387.6 ± 3.3
16	1000	20	63.17	74.89	0.013	0.0116	98.6	389.9 ± 4.6
17	1050	20	34.18	77.09	0.021	0.0239	100.0	382.8 ± 4.7
Sample IIa, $J = 0.002973 \pm 0.000023$								
1	500	20	9.53	219.87	0.169	0.5917	0.1	226.7 ± 42.7
2	600	20	18.22	115.59	0.034	0.1039	0.5	406.0 ± 16.9
3	700	20	79.90	92.11	0.024	0.0327	2.6	395.6 ± 4.1
4	750	20	93.80	88.75	0.019	0.0207	5.2	396.4 ± 3.6
5	800	20	461.95	85.03	0.017	0.0114	18.6	392.1 ± 2.8
6	825	20	811.46	82.53	0.015	0.0042	42.7	390.6 ± 2.8
7	835	20	539.73	82.78	0.015	0.0048	58.7	390.8 ± 2.8
8	840	20	245.61	83.67	0.015	0.0074	66.0	391.4 ± 2.9
9	850	20	165.88	84.08	0.018	0.0103	70.8	389.5 ± 3.1
10	875	20	171.66	83.75	0.015	0.0089	75.8	389.8 ± 3.1
11	900	20	212.19	83.71	0.016	0.0083	82.1	390.4 ± 2.9
12	925	20	248.27	83.21	0.016	0.0064	89.4	390.7 ± 2.8
13	950	20	266.39	83.45	0.014	0.0064	97.2	391.6 ± 2.9
14	975	20	66.46	87.04	0.016	0.0160	99.1	395.0 ± 3.7
15	1025	20	23.87	98.01	0.030	0.0582	99.7	388.5 ± 9.2
16	1100	20	15.03	130.88	0.045	0.1643	100.0	394.9 ± 22.1
Sample IIb, $J = 0.003346 \pm 0.000029$								
1	500	20	6.15	93.73	0.080	0.1269	0.3	311.1 ± 25.2
2	600	20	24.52	85.05	0.029	0.0516	1.4	378.8 ± 8.6
3	650	20	15.64	86.79	0.004	0.0369	2.1	408.2 ± 14.2
4	700	20	81.73	78.53	0.023	0.0328	6.3	374.0 ± 3.6
5	750	20	232.76	75.87	0.015	0.0206	18.6	378.6 ± 3.2
6	800	20	603.37	73.37	0.016	0.0131	51.4	377.2 ± 3.0
7	850	20	523.49	73.35	0.015	0.0127	80.0	377.7 ± 3.0
8	900	20	218.46	74.17	0.016	0.0178	91.8	374.3 ± 3.2
9	950	20	62.70	74.05	0.017	0.0184	95.1	372.8 ± 4.3
10	1000	20	39.73	74.75	0.017	0.0135	97.3	383.4 ± 5.8
11	1050	20	23.67	75.35	0.017	0.0153	98.5	383.7 ± 8.2
12	1150	20	28.17	76.36	0.021	0.0166	100.0	386.7 ± 6.7

Table 4. (Contd.)

no.	T, °C	t, min	^{40}Ar, 10^{-9} ncm^3	$^{40}Ar/^{39}Ar$	$^{38}Ar/^{39}Ar$	$^{36}Ar/^{39}Ar$	$\Sigma^{39}Ar$, %	Age, Ma ($\pm 1\sigma$)
Sample IIIa, $J = 0.003313 \pm 0.000029$								
1	450	20	1.73	135.88	0.414	0.3867	0.1	124.8 ± 120.0
2	550	20	5.39	107.72	0.132	0.1805	0.3	298.9 ± 13.4
3	600	20	4.55	86.64	0.062	0.0934	0.5	322.2 ± 8.8
4	650	20	11.91	83.12	0.040	0.0534	1.1	363.4 ± 11.2
5	700	20	20.31	81.32	0.022	0.0319	2.2	385.4 ± 4.0
6	725	20	23.85	78.16	0.021	0.0293	3.5	373.9 ± 4.3
7	750	20	40.16	77.68	0.021	0.0207	5.8	383.9 ± 4.1
8	775	20	117.95	74.58	0.018	0.0107	12.7	383.1 ± 3.4
9	800	20	160.46	73.32	0.018	0.0048	22.2	385.4 ± 3.2
10	825	20	336.54	72.63	0.015	0.0026	42.4	385.3 ± 3.1
11	850	20	307.00	72.74	0.014	0.0032	60.7	384.9 ± 3.1
12	875	20	205.37	72.95	0.016	0.0044	73.0	384.3 ± 3.1
13	900	20	155.64	73.27	0.016	0.0052	82.2	384.6 ± 3.1
14	925	20	149.93	73.27	0.016	0.0076	91.1	381.2 ± 3.0
15	950	20	97.88	73.39	0.016	0.0072	96.9	382.4 ± 3.1
16	1000	20	36.21	74.13	0.018	0.0131	99.1	377.5 ± 3.7
17	1100	20	16.60	76.23	0.015	0.0180	100.0	380.7 ± 5.8
Sample IVa, $J = 0.003246 \pm 0.000027$								
1	500	20	8.77	130.65	0.117	0.1899	0.2	390.9 ± 8.7
2	550	20	12.71	82.30	0.067	0.0630	0.7	339.0 ± 4.8
3	600	20	25.48	81.92	0.031	0.0325	1.7	380.4 ± 3.1
4	650	20	50.19	81.04	0.017	0.0332	3.7	375.3 ± 3.5
5	700	20	114.44	80.03	0.016	0.0208	8.3	387.9 ± 3.0
6	750	20	411.94	76.09	0.016	0.0073	25.7	388.0 ± 2.9
7	800	20	1078.99	74.36	0.019	0.0035	72.3	385.2 ± 2.9
8	850	20	407.26	75.46	0.016	0.0069	89.7	385.6 ± 3.1
9	900	20	161.83	75.25	0.018	0.0077	96.6	383.6 ± 3.5
10	950	20	39.83	76.99	0.021	0.0178	98.2	377.6 ± 4.1
11	1000	20	25.36	79.99	0.007	0.0217	99.2	386.3 ± 3.5
12	1100	20	21.05	89.67	0.031	0.0819	100.0	347.7 ± 3.3
Sample Va, $J = 0.002950 \pm 0.000022$								
1	500	20	15.15	156.87	0.102	0.2881	0.1	346.5 ± 30.5
2	600	20	29.52	103.94	0.023	0.0661	0.5	401.2 ± 9.3
3	650	20	49.95	93.64	0.024	0.0397	1.3	390.6 ± 4.2
4	700	20	112.26	89.21	0.020	0.0256	3.0	389.5 ± 3.1
5	750	20	136.45	86.11	0.019	0.0194	5.3	384.0 ± 3.2
6	800	20	873.41	83.24	0.016	0.0103	19.9	383.2 ± 2.7
7	850	20	885.38	81.67	0.015	0.0047	35.1	383.6 ± 2.7
8	900	20	439.34	81.80	0.016	0.0066	42.6	381.7 ± 2.7
9	500	20	481.15	81.71	0.015	0.0055	50.8	382.7 ± 2.8
10	600	20	148.31	83.79	0.017	0.0134	53.3	381.7 ± 3.0
11	650	20	275.89	82.16	0.017	0.0084	58.0	381.0 ± 2.6
12	700	20	266.71	82.19	0.016	0.0073	62.5	382.4 ± 2.6
13	750	20	301.57	82.12	0.016	0.0069	67.7	382.8 ± 2.6
14	800	20	299.60	82.19	0.016	0.0067	72.8	383.3 ± 2.6
15	850	20	356.82	82.26	0.016	0.0067	78.8	383.6 ± 2.8
16	900	20	554.49	81.91	0.015	0.0046	88.3	384.8 ± 2.8
17	950	20	434.46	81.80	0.015	0.0044	95.7	384.5 ± 2.8
18	1000	20	189.16	82.79	0.015	0.0060	98.9	386.8 ± 3.0
19	1050	20	45.57	87.93	0.016	0.0274	99.6	381.6 ± 4.4
20	1150	20	25.71	98.34	0.033	0.0284	100.0	424.8 ± 5.9

Table 4. (Contd.)

no.	*T*, °C	*t*, min	^{40}Ar, 10^{-9} ncm^3	$^{40}Ar/^{39}Ar$	$^{38}Ar/^{39}Ar$	$^{36}Ar/^{39}Ar$	$\Sigma^{39}Ar$, %	Age, Ma (±1σ)
Sample Vb, $J = 0.003181 \pm 0.000026$								
1	500	20	2.83	137.89	0.051	0.2824	0.1	288.1 ± 185.3
2	600	20	12.66	86.40	0.043	0.0614	0.9	354.5 ± 8.2
3	650	20	20.75	81.59	0.036	0.0337	2.2	370.4 ± 7.2
4	700	20	39.42	80.30	0.016	0.0159	4.7	388.7 ± 6.0
5	750	20	264.45	77.49	0.015	0.0103	22.1	383.5 ± 3.0
6	800	20	491.17	76.25	0.015	0.0055	55.0	384.4 ± 2.9
7	850	20	361.11	76.28	0.016	0.0063	79.2	383.3 ± 2.9
8	900	20	227.55	76.51	0.015	0.0060	94.4	384.8 ± 2.9
9	950	20	34.03	78.21	0.013	0.0132	96.6	382.8 ± 4.9
10	1000	20	20.20	80.05	0.018	0.0105	97.9	394.9 ± 5.5
11	1050	20	14.56	81.21	0.035	0.0268	98.8	378.1 ± 8.1
12	1150	20	18.98	82.64	0.029	0.0270	100.0	384.4 ± 4.9
Sample VIa, $J = 0.003149 \pm 0.000026$								
1	500	20	1.34	95.38	0.838	0.0769	0.3	371.7 ± 104.9
2	600	20	4.77	93.40	0.002	0.1041	1.4	324.8 ± 15.4
3	700	20	16.43	81.81	0.032	0.0327	5.6	369.3 ± 4.7
4	800	20	149.37	76.61	0.016	0.0133	46.5	371.8 ± 2.8
5	900	20	162.32	75.96	0.016	0.0085	91.3	375.3 ± 3.3
6	1000	20	15.08	77.12	0.017	0.0225	95.4	361.6 ± 5.5
7	1150	20	17.89	82.06	0.032	0.0300	100.0	374.2 ± 5.5
Sample VIb, $J = 0.002906 \pm 0.000022$								
1	500	20	12.25	324.26	0.203	0.8015	0.15	408.4 ± 45.3
2	600	20	21.50	137.93	0.062	0.1968	0.74	376.1 ± 11.0
3	700	20	64.59	95.11	0.022	0.0392	3.35	392.0 ± 4.2
4	750	20	69.09	88.66	0.010	0.0238	6.34	384.0 ± 3.6
5	800	20	274.67	85.86	0.017	0.0165	18.62	381.3 ± 2.7
6	825	20	521.81	82.38	0.015	0.0036	42.94	382.7 ± 2.7
7	835	20	273.98	82.69	0.016	0.0055	55.66	381.6 ± 2.7
8	845	20	160.67	83.78	0.016	0.0091	63.03	381.7 ± 2.8
9	875	20	142.62	83.40	0.017	0.0098	69.59	379.3 ± 2.9
10	900	20	182.92	83.62	0.015	0.0094	77.99	380.7 ± 2.8
11	950	20	315.12	83.84	0.017	0.0091	92.42	382.0 ± 2.7
12	1000	20	148.79	84.14	0.016	0.0092	99.21	383.2 ± 2.8
13	1100	20	22.13	107.04	0.026	0.0947	100.00	373.1 ± 11.8
Sample VIIa, $J = 0.003120 \pm 0.000025$								
1	450	20	3.31	403.14	0.166	1.1512	0.0	322.2 ± 182.7
2	550	20	11.74	113.50	0.055	0.1544	0.3	345.1 ± 20.8
3	600	20	16.50	108.89	0.036	0.1024	0.6	394.2 ± 8.2
4	650	20	33.22	92.92	0.034	0.0588	1.4	380.3 ± 4.0
5	675	20	35.25	91.19	0.027	0.0461	2.3	389.5 ± 3.4
6	700	20	42.36	88.35	0.021	0.0403	3.4	384.4 ± 3.5
7	725	20	59.30	83.32	0.021	0.0246	5.0	382.6 ± 4.0
8	750	20	69.69	82.10	0.016	0.0212	6.9	381.5 ± 4.1
9	775	20	145.88	80.55	0.016	0.0165	11.0	380.9 ± 3.2
10	800	20	460.01	77.65	0.016	0.0075	24.4	379.7 ± 2.8
11	825	20	700.63	76.52	0.015	0.0034	45.1	380.2 ± 2.8
12	850	20	543.04	76.61	0.015	0.0042	61.1	379.5 ± 2.8
13	875	20	333.06	76.68	0.015	0.0048	70.9	379.0 ± 2.8
14	900	20	290.28	77.38	0.015	0.0060	79.4	380.5 ± 2.8
15	950	20	466.06	76.78	0.015	0.0039	93.1	380.7 ± 2.8
16	1000	20	158.26	77.92	0.015	0.0076	97.7	380.9 ± 3.1
17	1050	20	37.34	79.61	0.014	0.0153	98.7	378.2 ± 4.6
18	1100	20	25.83	82.92	0.024	0.0343	99.4	367.6 ± 6.8
19	1150	20	21.52	85.81	0.024	0.0422	100.0	370.1 ± 5.9

Table 4. (Contd.)

no.	T, °C	t, min	^{40}Ar, 10^{-9} ncm^3	$^{40}Ar/^{39}Ar$	$^{38}Ar/^{39}Ar$	$^{36}Ar/^{39}Ar$	$\Sigma^{39}Ar$, %	Age, Ma ($\pm1\sigma$)
Sample VIIb, $J = 0.003084 \pm 0.000025$								
1	450	20	3.49	327.55	0.202	0.8936	0.02	322.8 ± 90.7
2	550	20	11.29	100.02	0.051	0.0842	0.26	376.3 ± 12.0
3	600	20	19.96	89.69	0.017	0.0372	0.73	392.2 ± 7.3
4	650	20	46.13	83.19	0.020	0.0207	1.90	385.0 ± 3.2
5	675	20	35.33	82.11	0.016	0.0148	2.81	388.0 ± 3.9
6	700	20	46.33	81.50	0.017	0.0178	4.01	381.2 ± 3.4
7	725	20	67.39	81.14	0.017	0.0165	5.76	381.4 ± 3.1
8	750	20	92.39	81.04	0.019	0.0187	8.16	378.0 ± 3.2
9	775	20	214.68	79.99	0.019	0.0146	13.83	378.7 ± 2.9
10	800	20	624.72	77.45	0.016	0.0053	30.85	379.6 ± 2.8
11	825	20	691.76	76.96	0.015	0.0034	49.81	380.0 ± 2.9
12	850	20	500.87	77.09	0.015	0.0037	63.52	380.1 ± 2.8
13	875	20	284.86	77.25	0.015	0.0039	71.30	380.5 ± 2.8
14	900	20	300.84	77.41	0.016	0.0048	79.50	380.1 ± 2.8
15	925	20	289.95	77.55	0.016	0.0046	87.39	381.0 ± 2.9
16	950	20	244.05	77.17	0.015	0.0038	94.06	380.3 ± 2.9
17	975	20	165.79	77.69	0.015	0.0023	98.56	384.7 ± 3.2
18	1000	20	31.28	80.58	0.016	0.0188	99.38	375.7 ± 5.2
19	1050	20	13.53	84.72	0.041	0.0398	99.72	366.3 ± 4.8
20	1150	20	12.14	89.99	0.042	0.0447	100.00	383.6 ± 4.1
Sample VIIIa, $J = 0.002880 \pm 0.000022$								
1	500	20	26.07	208.46	0.102	0.4202	0.1	392.6 ± 12.5
2	600	20	52.38	107.97	0.031	0.0842	0.7	387.6 ± 5.1
3	650	20	69.05	95.33	0.024	0.0328	1.5	398.2 ± 4.3
4	700	20	148.91	89.43	0.017	0.0183	3.4	391.5 ± 2.9
5	725	20	142.95	87.90	0.017	0.0170	5.3	386.7 ± 3.1
6	750	20	173.79	88.90	0.018	0.0219	7.6	384.8 ± 2.9
7	775	20	352.84	88.71	0.018	0.0200	12.1	386.4 ± 2.7
8	800	20	962.67	84.67	0.016	0.0069	25.2	385.6 ± 2.7
9	810	20	774.69	83.77	0.015	0.0036	35.8	386.0 ± 2.7
10	815	20	506.23	84.09	0.015	0.0052	42.7	385.3 ± 2.7
11	820	20	376.60	84.25	0.016	0.0062	47.9	384.7 ± 2.8
12	825	20	323.01	84.59	0.016	0.0066	52.2	385.6 ± 2.8
13	835	20	262.90	84.57	0.015	0.0073	55.8	384.7 ± 2.7
14	800	20	101.62	86.18	0.015	0.0143	57.2	382.8 ± 3.3
15	800	20	73.64	87.99	0.018	0.0167	58.1	387.4 ± 3.6
16	850	20	185.55	84.60	0.016	0.0077	60.6	384.3 ± 2.8
17	875	20	335.19	84.37	0.015	0.0065	65.2	384.9 ± 2.7
18	900	20	409.03	84.44	0.015	0.0060	70.8	385.8 ± 2.8
19	925	20	613.15	84.21	0.015	0.0047	79.1	386.4 ± 2.7
20	940	20	633.73	84.22	0.015	0.0044	87.8	386.8 ± 2.7
21	950	20	369.56	84.49	0.015	0.0045	92.8	387.8 ± 2.8
22	960	20	245.41	84.67	0.016	0.0058	96.1	387.0 ± 2.8
23	980	20	188.70	85.18	0.015	0.0050	98.7	390.1 ± 2.9
24	1010	20	87.41	87.88	0.016	0.0201	99.8	382.8 ± 3.3
25	1050	20	17.60	108.08	0.028	0.1094	100.0	356.5 ± 15.1
Sample VIIIb, $J = 0.003053 \pm 0.000024$								
1	450	20	2.10	310.05	0.392	1.0295	0.03	31.8 ± 143.3
2	550	20	6.19	111.28	0.051	0.1371	0.25	353.0 ± 18.9
3	600	20	9.82	99.52	0.029	0.0763	0.65	380.9 ± 6.1
4	650	20	18.84	86.68	0.035	0.0248	1.54	391.5 ± 3.8
5	675	20	20.60	85.99	0.021	0.0290	2.51	382.9 ± 4.1
6	700	20	23.55	83.18	0.020	0.0207	3.66	381.3 ± 4.3
7	725	20	29.26	82.95	0.021	0.0198	5.10	381.5 ± 5.1
8	750	20	40.17	82.06	0.019	0.0222	7.09	374.3 ± 3.8
9	775	20	91.18	81.90	0.019	0.0216	11.61	374.4 ± 2.9
10	800	20	252.70	78.42	0.015	0.0065	24.71	378.8 ± 2.8
11	825	20	351.92	77.55	0.015	0.0037	43.16	378.6 ± 2.8
12	850	20	266.21	77.62	0.015	0.0050	57.10	377.1 ± 2.8
13	900	20	301.71	77.42	0.014	0.0044	72.94	377.1 ± 2.9
14	950	20	306.94	77.95	0.015	0.0037	88.95	380.4 ± 2.8
15	1000	20	194.44	78.32	0.015	0.0037	99.04	382.1 ± 3.0
16	1050	20	19.66	83.42	0.023	0.0271	100.00	373.9 ± 5.0

Note: J is a parameter characterizing the neutron flux.

Table 5. Results of $^{40}Ar/^{39}Ar$ glaucophane dating

no.	*T*, °C	*t*, min	^{40}Ar, 10^{-9} ncm^3	$^{40}Ar/^{39}Ar$	$^{38}Ar/^{39}Ar$	$^{37}Ar/^{39}Ar$	$^{36}Ar/^{39}Ar$	Ca/K	$\Sigma^{39}Ar$, %	Age, Ma (±1σ)
Sample I, $J = 0.003620 \pm 0.000034$										
1	600	15	2.02	381.33	0.486	16.39	1.098	29.3	1.1	336.8 ± 265.6
2	800	15	6.54	122.04	0.112	0.07	0.148	0.1	12.4	450.5 ± 22.9
3	900	15	28.79	99.56	0.060	1.69	0.072	3.0	73.5	449.6 ± 5.9
4	1200	20	15.57	123.91	0.054	1.27	0.156	2.3	100.0	446.9 ± 20.2
Sample IIIa, $J = 0.003548 \pm 0.000033$										
1	600	20	1.66	520.57	1.000	362.12	1.732	646.4	0.4	55.2 ± 238.4
2	800	20	4.02	138.00	0.125	196.58	0.269	350.9	4.5	340.4 ± 45.7
3	900	20	12.53	85.58	0.046	17.47	0.056	31.2	24.7	395.3 ± 7.2
4	1000	20	36.70	79.67	0.058	74.77	0.034	133.5	88.3	397.7 ± 4.3
5	1170	20	6.91	81.70	0.039	65.70	0.060	117.3	100.0	369.0 ± 10.2
Sample IVa, $J = 0.003480 \pm 0.000032$										
1	600	20	1.42	305.26	0.464	316.56	0.748	565.1	0.4	463.4 ± 273.6
2	800	20	4.24	109.18	0.111	167.32	0.177	298.7	4.5	326.0 ± 22.9
3	900	20	20.74	77.57	0.037	13.16	0.031	24.3	24.7	385.3 ± 4.0
4	1170	20	61.11	75.43	0.035	11.18	0.020	20.0	88.3	391.2 ± 3.5
Sample Vb, $J = 0.003412 \pm 0.000030$										
1	800	20	2.16	171.27	0.129	3.254	0.333	5.81	7.7	400.2 ± 99.2
2	900	20	9.92	112.51	0.089	3.059	0.121	5.46	61.4	419.3 ± 13.8
3	950	20	4.96	101.95	0.038	5.367	0.097	9.58	91.0	403.0 ± 36.2
4	1200	20	4.15	281.25	0.087	4.664	0.623	8.32	100.0	516.9 ± 87.9

Note: *J* is a parameter characterizing the neutron flux.

multiple regression equation, we obtain the following calculated minimum and maximum age values for the garnet glaucophanite and omphacite–garnet rock, respectively: $t_{Grt\text{-}Gl}$ = 390.7 Ma (Al_{min} = 2.1 f.u., a_{max} = 0.776 mm) and $t_{Omp\text{-}Grt}$ = 374.4 Ma (Al_{max} = 2.45 f.u., a_{min} = 0.10 mm). It is worth noting that the minimum age value for the omphacite-garnet rock coincides with the phengite age for the eclogites obtained previously by other researchers (Beane and Connelly, 2000; Matte *et al.*, 1993; Lennykh *et al.*, 1995).

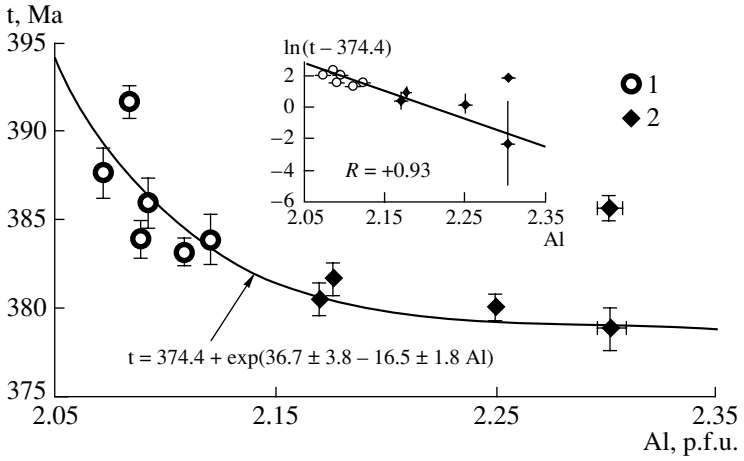

Fig. 7. Dependence of the measured $^{40}Ar/^{39}Ar$ age of phengite *t* on its Al concentration.
(1) Garnet glaucophanite; (2) omphacite–garnet rock. The inset shows the correlation between ln (t – 374.4) and the Al concentration, *R* is the correlation coefficient.

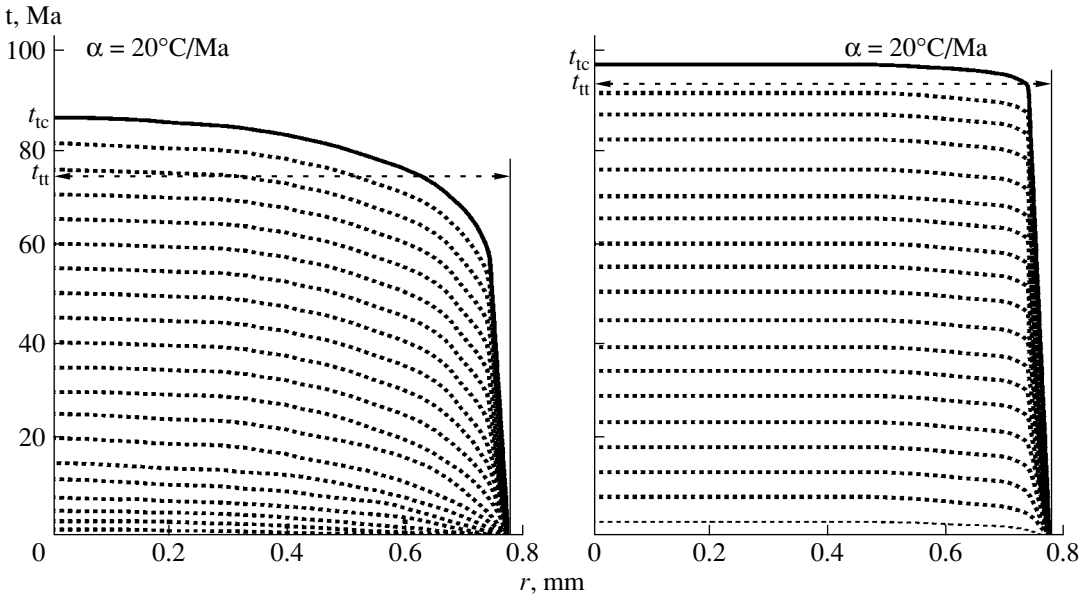

Fig. 8. Results of the numerical simulation of the distribution of effective age in a phengite flake with a radius $r = 0.776$ mm during the linear cooling at a rate α equal to 2.5 and 20°C/m.y. The trajectories are drawn with a step of 5 m.y. Arrows indicate the age values at the center of the flakes and the total fusion age values for the latest trajectories.

The ages of glaucophane IIIa, IVa, and Vb (Table 3, Fig. 4) lie within the range of 387–411 Ma and are consistent (with regard for the errors) with the maximum measured and calculated phengite ages. The age values yielded by glaucophane I are much older. There can be two possible explanations of this phenomenon. The variations in the measured age can be caused by the presence of excess radiogenic Ar in the glaucophane. If this hypothesis proves true, then the least perturbed age is 388.6 ± 3.5 Ma, which was yielded by glaucophane IVa and which coincides with the three oldest phengite dates (samples I, II, and VIIIa). With regard for the fact that the closure temperature of the K/Ar system in amphibole (Harrison, 1981; Lister and Baldwin, 1996) is comparable with the temperature of the high-temperature crystallization of the minerals (about 500–550°C), this date can be considered the closest to the age of the final metamorphic stage.

At the same time, the variations in the measured glaucophane age can correspond to the actual duration of the metamorphic event (from 411 to 389 Ma). This situation does not allows for an unambiguous interpretation of the glaucophane I date (449.0 ± 5.9 Ma).

By analogy with muscovite, whose closure temperature of the K/Ar system was constrained experimentally (Robbins, 1972; McDougall and Harrison, 1988; Lister and Baldwin, 1996) at 350–450°C, the phengite dates can be regarded as the "cooling" ages. In this situation, the age of the high-pressure metamorphism should be close to the estimates obtained for the largest phengite flakes from the garnet glaucophanite (392 Ma), and the phengite dates from the omphacite–garnet rock (378 Ma) should correspond to the cooling of the rocks to temperatures below 350°C during exhumation. Taking into considerations the dependences presented above for the phengite age and the size of its flakes, the limiting age estimates are 390.7–374.5 Ma.

In order to determine the quantitative parameters of the thermal history of the rock sample in question, we numerically simulated the behavior of the K/Ar system in the phengite based on the mechanism of ^{40}Ar volumetric diffusion in compliance with the second Fick law and with regard for the origin of ^{40}Ar in this mineral via the radioactive decay of K

$$\delta c/\delta t = D\nabla^2 c + \lambda[^{40}K]_0 \exp(-\lambda t),$$

where c is the concentration of radiogenic Ar, D is the diffusion coefficient, ∇ is the concentration gradient, λ is the decay rate of ^{40}K, and $[^{40}K]_0$ is the initial K concentration. Argon diffusion through phengite flakes is adequately described within the scope of cylindrical geometry, with the above equation acquiring the form

$$\delta c/\delta t = D(\delta^2 c/\delta r^2 + 1/r\delta c/\delta r) + \lambda[^{40}K]_0 \exp(-\lambda t),$$

where r is the distance to the center of the flake. The dependence of the diffusion coefficient on temperature is determined by the Arrhenius equation

$$D = D_0 \exp(-E/RT),$$

where D_0 is the preexponential factor, E is the activation energy, R is the gas constant, and T is the absolute temperature. The simulation was conducted with the use of the Diffarg program complex (Wheeler, 1996). The temporal variations in the concentration profiles for diffusing radiogenic Ar in minerals were calculated

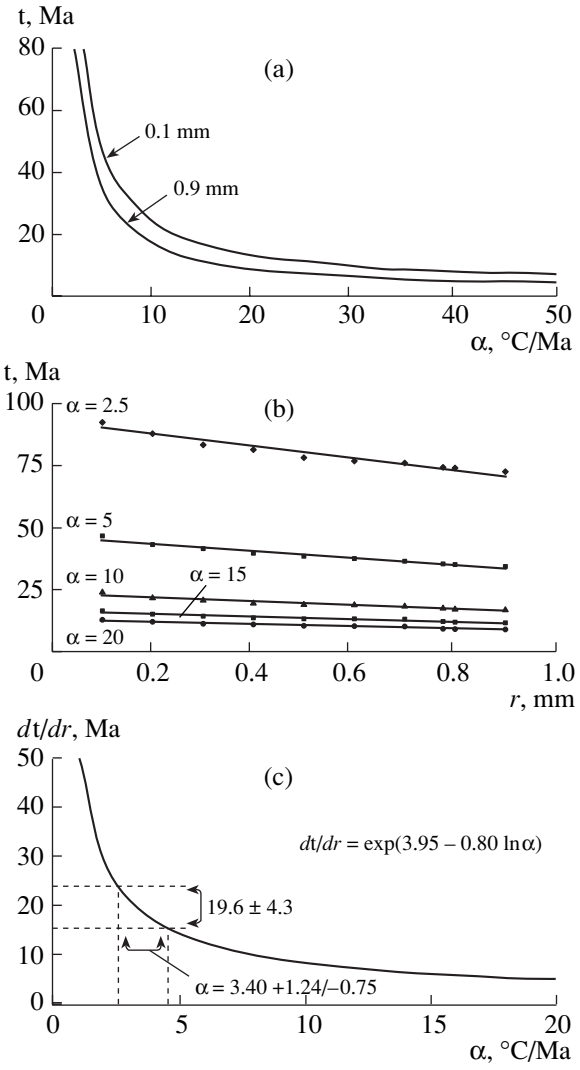

Fig. 9. (a) Dependence of the time span that had elapsed from the onset of linear cooling from a temperature of 600°C to the complete closure of the isotopic system on the cooling rate α for flakes 0.1 and 0.9 mm in size.

(b) Dependence of the closure time of the phengite isotopic system on the sizes of its flakes.

(c) Dependence of the age derivative with respect to the flake sizes ($dt/d\alpha$ is the slope of the line in Fig. 9b) on the cooling rate α.

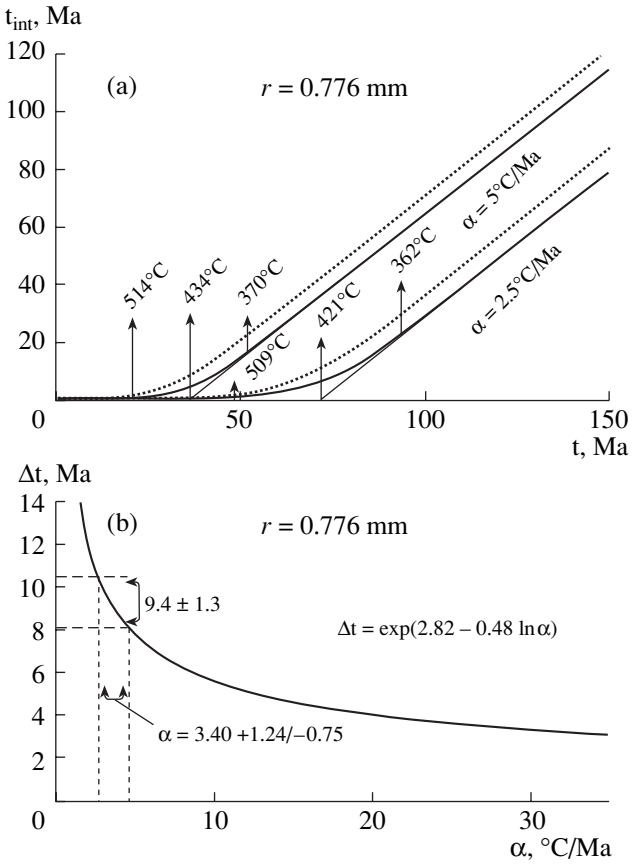

Fig. 10. (a) Dependence of the model total fusion age of phengite flakes 0.776 mm in radius on time (the starting moment corresponds to a temperature of 600°C) at linear cooling with a rate of 2.5 and 5°C/Ma Dotted lines are model age lines at the centers of the flakes. The diagrams show the temperatures of the beginning of the partial accumulation of radiogenic Ar, closure temperatures according to (Dodson, 1973), and temperatures below which the losses of radiogenic Ar become negligibly small.

(b) Dependence of the difference Δt between the age values for the central part of a phengite flake 0.776 mm in radius and its total fusion age on the linear cooling rate α.

with the use of the finite difference technique, which is based on the Crank–Nicolson method (Press *et al.*, 1986). The calculations were carried out with the use of the kinetic parameters of Ar diffusion in muscovite (E = 52.3 kcal/mol, $D_0 = 5 \times 10^{-2}$ cm^2/s), which were quantified in hydrothermal experiments (McDougall and Harrison, 1988).

We considered the linear cooling of the system with rates ranging from 2.5 to 50°C/m.y., at a zero boundary condition throughout the whole time interval in question. As an illustrative example, Fig. 8 exhibits the profiles of radiogenic Ar distribution that were calculated in the form of an effective age for a phengite flake 0.776 mm in radius (which corresponds to the maximum measured dimension a of phengite flakes), a cooling rate of 2.5 and 20°C/m.y., and a time step of 5 m.y.

The simulation was conducted for phengite flakes from 0.1 to 0.9 mm in radius. Figure 9a illustrates the dependence of the time that had elapsed from the beginning of linear cooling (T_0 = 600°C) until the complete closure of the system on the cooling rate. The correlation between the time and flake radius is linear (Fig. 9b), and the slope of the lines (dt/dr) decreases with increasing cooling rate, with this dependence described by the equation (Fig. 9c)

$$dt/dr = \exp(3.95–0.80\ln\alpha),$$

where α is the cooling rate. As follows from the derived dependences of the measured age values on the half-

length of the short axis of phengite flakes (Fig. 6), the derivative of the age with respect to the flake size is equal to 19.6 ± 4.3 m.y./mm. Substituting this value into the formula, one can evaluate the cooling rate, which is equal to 3.40 –0.75/+1.24°C/m.y. For the modern thermal gradient of 10°C/km, this value corresponds to an exhumation velocity of 0.34 –0.075/+0.124 mm/yr.

Argon conservation began much earlier in the central portions of phengite flakes than in their peripheral parts. For example, during linear cooling at a rate of 5°C/m.y., Ar starts to accumulate in the central part of a flake 0.776 mm in radius at 514°C (Fig. 10a), and the final closure of the isotopic system occurs at 370°C. With regard for the aforesaid, the age of the central part of the flake should be the closest to the crystallization age of the metamorphic minerals. For the concentration profiles reconstructed by means of numerical simulations (Fig. 8), one can determine the difference between the age value for the central part of a flake and its total fusion age. The dependence of this difference on the cooling rate of the flake 0.776 mm in radius is presented in Fig. 10b. It is described by an equation analogous to the dependence of the age derivative with respect to the flake radius (Fig. 9c). Substituting the cooling rate into this equation, one can obtain the difference between the total fusion age and the age in the central part of the grain. For a flake 0.776 m in radius, this difference is equal to 9.4 ± 1.3 m.y. In our case, the morphology of phengite flakes more resembles an ellipse. It is logical to hypothesize that the difference between the total fusion age of such a flake and its age at the center should be no less than the analogous difference in cylindrical geometry if the cylinder radius is equal to the half-length of the short axis of the ellipse. Correspondingly, while a total fusion age of 390.7 Ma was obtained for a flake whose short-axis half-length is equal to 0.776 mm, the age in the central portion of this flake should be no younger than 400 ± 1.3 Ma. This means that the crystallization age of the metamorphic minerals is no younger than 400 Ma.

CONCLUSIONS

Our $^{40}Ar/^{39}Ar$ dating with stepwise heating of phengite from the contact zone of garnet glaucophanite and omphacite–garnet rock (eclogite) has demonstrated that the behavior of the K/Ar system of phengite is controlled by the mechanism of volumetric diffusion. The maximum age values of 392 Ma were measured in the garnet glaucophanite away from the contact. The results of numerical simulation indicate that the high-pressure metamorphism is no younger than 400 Ma. For the situation of linear cooling, the cooling rate should have been 3.40 –0.75/+1.24°C/m.y., which corresponds to an exhumation velocity of the metamorphic rocks equal to 0.34 mm/yr. Note that this value is consistent with the data obtained by other methods (Leech and Stockli, 2000) and constrains the maximum exhumation velocity at 0.46 mm/yr. More precise estimates require the application of independent methods for the reconstruction of the thermal history of the metamorphic rocks. In this context, interesting minerals are phases of variable composition with chemical zoning, first of all, garnet crystals. In our sample, all of them are zonal and, thus, will be used for estimating the duration of metamorphism and the *P* and *T* variation rates during the prograde and retrograde metamorphic stages.

The high-pressure metamorphic age estimated by phengite is consistent with the dates yielded by glaucophane from three samples: 389–411 Ma.

The relations identified in the rocks make it possible to explain the scatter of the $^{40}Ar/^{39}Ar$ dates obtained by other researchers (Beane and Connelly, 2000; Matte *et al.*, 1993; Lennykh *et al.*, 1995). Regretfully, they do not present any information of the sizes of phengite flakes and their compositions, and this precludes the more comprehensive analysis of the published data and their comparison with our results.

Bearing in mind that the mobility of the Rb/Sr system in phengite is comparable with the mobility of the K/Ar system, the dating of the omphacite–garnet rock by the $^{40}Ar/^{39}Ar$ method provides a new look at the results of the Rb/Sr dating of eclogites (Glodny *et al.*, 2002). The Rb/Sr age values (372–378.5 Ma) are comparable with the Ar/Ar dates.

ACKNOWLEDGMENTS

This study was supported by the Russian Foundation for Basic Research, project nos. 05-05-64317 and 05-05-64438.

REFERENCES

1. R. J. Beane and J. N. Connelly, "$^{40}Ar/^{39}Ar$, U/Pb, and Sm–Nd Constraints on the Timing of Metamorphic Events in the Maksyutov Complex, Southern Ural Mountains," J. Geol. Soc. **157**, 811–822 (2000).
2. R. J. Beane, J. G. Liou, R. G. Coleman, and M. L. Leech, "Petrology and Retrograde *P–T* Path for Eclogites of the Maksyutov Complex, Southern Ural Mountains, Russia," The Island Arc **4**, 254–266 (1995).
3. B. V. Chesnokov and V. A. Popov, "Increasing Volume of Quartz Grains in the Eclogites of Southern Urals," Dokl. Akad. Nauk SSSR **162** (4), 909–910 (1965).
4. N. L. Dobretsov and L. V. Dobretsova, "New Mineralogical Data on the Maksyutov Eclogite–Glaucophane Schist Complex," Dokl. Akad. Nauk SSSR **294** (2), 375–380 (1988).
5. N. L. Dobretsov, "Structural Evolution of the Urals, Kazakhstan, Tien Shan, and Altai–Sayan Region in the Ural–Mongolian Foldbelt" Geol. Geofiz. **44** (1–2), 5–27 (2003).
6. N. L. Dobretsov, V. S. Shatsky, R. G. Coleman, *et al.*, "Tectonic Setting and Petrology of Ultrahigh-Pressure Metamorphic Rocks in the Maksyutov Complex, Ural Mountains, Russia," Int. Geol. Rev. **38**, 136–160 (1996).

7. M. H. Dodson, "Closure Temperature in Cooling Geochronological and Petrological Systems," Contrib. Mineral. Petrol. **40**, 259–274 (1973).
8. J. Glodny, B. Bingen, H. Austrheim, *et al.*, "Precise Eclogitization Ages Deduced from Rb/Sr Mineral Systematics: The Maksyutov Complex, Southern Urals, Russia," Geochim. Cosmochim. Acta **66** (7), 1221–1235 (2002).
9. T. M. Harrison, "Diffusion of ^{40}Ar in Hornblende," Contrib. Mineral. Petrol. **78** (3), 324–331 (1981).
10. R. Hetzel, H. P. Echtler, W. Seifert, *et al.*, "Subduction- and Exhumation-Related Fabrics in the Paleozoic High-Pressure–Low-Temperature Maksyutov Complex, Antingan Area, Southern Urals, Russia," Bull. Geol. Soc. Am. **110**, 916–930 (1998).
11. T. J. B. Holland and R. Powell, "An Internally Consistent Thermodynamic Dataset for Phases of Petrological Interest," J. Metam. Geol. **16**, 309–343 (1998).
12. M. L. Leech and D. F. Stockli, "The Late Exhumation History of the Ultrahigh-Pressure Maksyutov Complex, South Ural Mountains, from New Apatite Fission Track Data," Tectonics **19** (1), 153–167 (2000).
13. M. L. Leech and W. G. Ernst, "Graphite Pseudomorphs After Diamond? A Carbon Isotope and Spectroscopic Study of Graphite Cuboids from the Maksyutov Complex, South Ural Mountains, Russia," Geochim. Cosmochim. Acta **62**, 2143–2154 (1998).
14. M. L. Leech, E. P. Metzger, J. L. Wooden, *et al.*, "New Eclogitization and Protolith Ages for the Maksyutov Complex (South Ural Mountains) Based on U–Pb Zircon SHRIMP Data," EOS Trans. Am. Geophys. Union **83**, F1245 (2002).
15. V. I. Lennykh, P. M. Valizer, R. Beane, *et al.*, "Petrotectonic Evolution of the Maksyutov Complex, Southern Urals, Russia: Implications for Ultrahigh-Pressure Metamorphism," Int. Geol. Rev. **37**, 584–600 (1995).
16. G. S. Lister and S. L. Baldwin, "Modeling the Effect of Arbitrary *P–T–t* Histories on Argon Diffusion in Minerals Using the Mac Argon Program for the Apple Macintosh," J. South Am. Earth Sci. **253**, 83–109 (1996).
17. P. Matte, H. Maluski, R. Caby, *et al.*, "Geodynamic Model and ^{40}Ar/^{39}Ar Dating for the Generation and Emplacement of the High Pressure (HP) Metamorphic Rocks in SW Urals," C. R. Acad. Sci., Ser. II **317**, 1667–1674 (1993).
18. I. McDougall and T. M. Harrison, *Geochronology and Thermochronology by the ^{40}Ar/^{39}Ar Method* (Oxford Univ. Press, Oxford, 1988).
19. W. H. Press, B. P. Flannery, S. A. Teukolsky, and W. T. Vetterling, *Numerical Recipes in Pascal* (Cambridge Univ. Press, Cambridge, 1986).
20. V. N. Puchkov, "Structure and Geodynamics of the Uralian Orogen," in *Orogeny Through Time*, Ed. by J.-P. Burg and M. Ford, Geol. Soc. Spec. Publ. **121**, 201–236 (1997).
21. G. A. Robbins, M. Sci. Thesis (Brown Univ., 1972).
22. B. A. Schulte and P. Blümel, "Metamorphic Evolution of Eclogite and Associated Garnet–Mica Schist in the High-Pressure Metamorphic Maksyutov Complex, Ural, Russia," Geol. Rundsch. **87**, 561–576 (1999).
23. V. S. Shatsky, E. Jagoutz, and O. A. Koz'menko, "Sm–Nd Dating of the High-Pressure Metamorphism of the Maksyutov Complex, Southern Urals," Dokl. Akad. Nauk **352** (6), 285–288 (1997) [Dokl. Earth Sci. **352** (2), 285–288 (1997)].
24. N. I. Volkova, A. E. Frenkel, V. I. Budanov, and G. G. Lepezin, "Geochemical Signatures for Eclogite Protolith from the Maksyutov Complex, South Urals," J. Asian Earth Sci. **23**, 745–759 (2004).
25. J. Wheeler, "Diffarg: A Program for Simulating Argon Diffusion Profiles in Minerals," Comput. Geosci. **22** (8), 919–929 (1996).
26. L. P. Zonenshain, V. G. Korinevsky, D. M. Kazmin, *et al.*, "Plate Tectonic Model of the South Urals Development," Tectonophysics **109**, 95–135 (1984).